Amino Acids
DOI 10.1007/s00726-010-0759-0

ORIGINAL ARTICLE

Zinc induces disorder-to-order transitions in free and membrane-associated *Thellungiella salsuginea* dehydrins TsDHN-1 and TsDHN-2: a solution CD and solid-state ATR-FTIR study

Luna N. Rahman · Vladimir V. Bamm · Janine A. M. Voyer · Graham S. T. Smith · Lin Chen · Mahmoud W. Yaish · Barbara A. Moffatt · John R. Dutcher · George Harauz

Received: 14 June 2010 / Accepted: 21 September 2010

Abstract Dehydrins are intrinsically unstructured proteins that are expressed in plants experiencing extreme environmental conditions such as drought or low temperature. Although their role is not completely understood, it has been suggested that they stabilize proteins and membrane structures during environmental stress and also sequester metals such as zinc. Here, we investigate two dehydrins (denoted as TsDHN-1 and TsDHN-2) from *Thellungiella salsuginea*. This plant is a crucifer that thrives in the Canadian sub-Arctic (Yukon Territory) where it grows on saline-rich soils and experiences periods of both extreme cold and drought. We show using circular dichroism and attenuated total reflection-Fourier transform infrared spectroscopy that ordered secondary structure is induced and stabilized in these proteins, both in free and vesicle-bound form, by association with zinc. In membrane-associated form, both proteins have an increased proportion of β-strand conformation induced by the cation, in addition to the amphipathic α-helices formed by their constituent K-segments. These results support the hypothesis that dehydrins stabilize plant plasma and organellar membranes in conditions of stress, and further that zinc may be an important co-factor in stabilization. Whereas dehydrins in the cytosol of a plant cell undergoing dehydration or temperature stress form bulk hydrogels and remain primarily disordered, dehydrins with specific membrane- or protein-associations will have induced ordered secondary structures.

L. N. Rahman · V. V. Bamm · J. A. M. Voyer · G. S. T. Smith · L. Chen · M. W. Yaish · G. Harauz (✉)
Department of Molecular and Cellular Biology, University of Guelph, 50 Stone Road East, Guelph, ON N1G 2W1, Canada
e-mail: gharauz@uoguelph.ca

L. N. Rahman · V. V. Bamm · J. A. M. Voyer · G. S. T. Smith · L. Chen · J. R. Dutcher · G. Harauz
Biophysics Interdepartmental Group, University of Guelph, Guelph, ON N1G 2W1, Canada

L. Chen · J. R. Dutcher
Department of Physics, University of Guelph, Guelph, ON N1G 2W1, Canada

M. W. Yaish · B. A. Moffatt
Department of Biology, University of Waterloo, Waterloo, ON N2L 3G1, Canada

Present Address:
M. W. Yaish
Department of Biology, College of Science, Sultan Qaboos University, 123 Muscat, P.O. Box 36, Muscat, Oman

Keywords Dehydrins · Late embryogenesis abundant (LEA) · Cold tolerance · Drought tolerance · Intrinsically-disordered protein · Induced folding · Poly-proline type II · CD spectroscopy · FTIR spectroscopy · ATR-FTIR spectroscopy

Abbreviations

ATR	Attenuated total reflection
CD	Circular dichroism spectroscopy
Chol	Cholesterol
TsDHN-1	Acidic *Thellungiella salsuginea* dehydrin 1
TsDHN-2	Basic *Thellungiella salsuginea* dehydrin 2
ddH_2O	Distilled, deionised water
DGDG	Digalactosyldiacylglycerol
DMPG	1, 2-dimyristoyl-*sn*-glycero-3-[phospho-*rac*-(1-glycerol)]
FTIR	Fourier transform infrared
HCA	Hydrophobic cluster analysis
IDP	Intrinsically disordered protein

Published online: 06 October 2010

LEA	Late embryogenesis abundant
MGDG	Monogalactosyldiacylglycerol
PC	Phosphatidylcholine
PE	Phosphatidylethanolamine
PI	Phosphatidylinositol
PPII	Poly-proline type II conformation
PS	Phosphatidylserine
SQDG	Sulfoquinovosyl diacylglycerol

Introduction

Many plants have evolved with the ability to withstand environmental stresses such as low temperature and drought. Some plants respond to these stresses by inducing genes that encode the late embryogenesis-abundant (LEA) proteins (Battaglia et al. 2008; Caramelo and Iusem 2009; Hundertmark and Hincha 2008). Most LEA proteins are intrinsically disordered proteins (IDPs, also referred to as intrinsically unstructured proteins; Eom et al. 1996; Goldgur et al. 2007; Hundertmark and Hincha 2008; Lisse et al. 1996; Mouillon et al. 2006; Soulages et al. 2003; Thalhammer et al. 2010; Tompa and Kovacs 2010). Such proteins are distinguished by their lack of a defined tertiary fold, but they adopt altered conformations in association with other molecules or under different environmental conditions (Mohan et al. 2009; Uversky 2009; Vucetic et al. 2007; Xie et al. 2007a, b). The way in which LEA proteins protect plants from environmental stress is not completely understood, although numerous mechanisms have been described (Battaglia et al. 2008; Rajesh and Manickam 2006; Tunnacliffe and Wise 2007; Wise and Tunnacliffe 2004). Amongst many macromolecular associations, LEA proteins have been suggested to stabilize plasma and organellar membranes (Beck et al. 2007; Danyluk et al. 1998; Han et al. 1997; Hincha et al. 1990; Ismail et al. 1999; Puhakainen et al. 2004; Steponkus et al. 1998; Thalhammer et al. 2010; Tolleter et al. 2007, 2010; Zhang et al. 2010). This current study is performed within the theme of membrane-stabilization by particular LEA proteins called dehydrins.

Dehydrins: intrinsically disordered group 2 LEA proteins

The group 2 LEA proteins are also known as dehydrins (Allagulova et al. 2003; Battaglia et al. 2008; Beck et al. 2007; Campbell and Close 1997; Close 1997; Garay-Arroyo et al. 2000; Kosova et al. 2007, 2008; Mouillon et al. 2006; Puhakainen et al. 2004; Zhu et al. 2000). Dehydrins contain three conserved sequences: the K-segment, a lysine-rich domain that has the potential for electrostatic and hydrophobic interactions with membranes attributed to the formation of amphipathic α-helices (Allagulova et al. 2003; Bravo et al. 2003; Campbell and Close 1997; Close 1997; Koag et al. 2003, 2009; Rorat et al. 2006); the S-segment, a serine-rich domain which may be phosphorylated, modulating the dehydrin protein's ability to bind ligands such as metal ions (Alsheikh et al. 2003; Heyen et al. 2002); and the Y-segment, which is found at the N-terminus and is similar to the nucleotide-binding sites of plant and bacterial chaperone proteins (Allagulova et al. 2003; Battaglia et al. 2008; Campbell and Close 1997; Close 1997; Jepson and Close 1995). Dehydrins can be categorised into different classes based on their combination of K, S, and Y segments, and some are interspersed with φ segments. On this basis, several major classes have been previously described (K_n, SK_n, K_nS, Y_nSK_2, and Y_2K_n) (Allagulova et al. 2003; Battaglia et al. 2007; Campbell and Close 1997; Close 1997).

Dehydrins in the cytosol of plant cells form highly stable hydrated gels and remain primarily disordered (Mouillon et al. 2008; Tompa et al. 2006; Wolkers et al. 2001). However, the K-segment forms an amphipathic α-helix that can associate with membrane surfaces (Allagulova et al. 2003; Rorat et al. 2006). Association of dehydrins with detergents and lipids can lead to ordered secondary structure (Ceccardi et al. 1994; Ismail et al. 1999; Koag et al. 2003, 2009; Kovacs et al. 2008; Rahman et al. 2010; Soulages et al. 2002; Soulages et al. 2003). (See also reference (Thalhammer et al. 2010) which is a study of intrinsically disordered group 3 LEA proteins interacting with lipid membranes, and reference (Tolleter et al. 2010) on a mitochondrial LEA protein.) Citrus dehydrins are known to have a scavenging role against hydroxyl and peroxyl radicals that are generated in plants during environmental stress (Hara et al. 2004; Ueda et al. 2003), a role that has been suggested to involve metal- and DNA-binding (Hara et al. 2005, 2009; Kalifa et al. 2004; Rom et al. 2006). The metals reported to interact with citrus dehydrins, by virtue of histidine-rich domains, are Fe^{3+}, Co^{2+}, Ni^{2+}, Cu^{2+}, and Zn^{2+}, but not Mg^{2+}, Ca^{2+}, and Mn^{2+} (Hara et al. 2005). However, Ca^{2+}-binding has been reported for other dehydrins and shown to depend on their phosphorylation state (Alsheikh et al. 2003; Heyen et al. 2002). In general, then, the associations of dehydrins with Ca^{2+} and Zn^{2+} appear to be the most physiologically significant, and we focus on the latter cation in this study (Goldgur et al. 2007; Hara et al. 2005, 2009; Rom et al. 2006).

Thellungiella salsuginea dehydrins

We report here on studies of two dehydrin proteins TsDHN-1 and TsDHN-2 derived from the plant *Thellungiella salsuginea* (salt-lick mustard, saltwater cress; also called

A Acidic dehydrin TsDHN-1

```
  1  MAEEYKNASE EFKNVPEHET TPKISTTEEP SAEVKDRGFF DFLGKKKEEV
 51  KPQETTTPLE SEFEHKAQIS EPPAFVAKHE EEQETKENKP TLVEQLHQKH
101  VEEEENKPSL FDKLHRSSSS SSSSSDEEGE DGEKRKKKKE KKKTVEGEDK
151  TEEENKGVMD KIKEKFPHAK KTEDDHAPVV TGVPETEKIG MTEKIKEKLP
201  GHGKKPEDSP VVDTAPVVET ATPITAEHSA EHPAENKGFL EKIKEKLPGH
251  HAKGTEEMEK KEKESDA
```

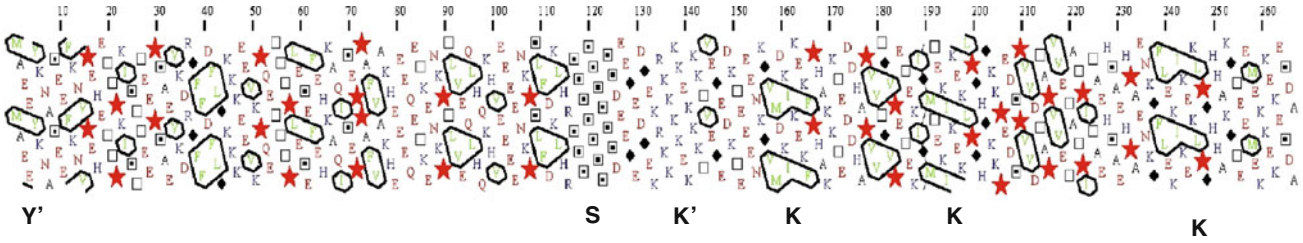

B Basic dehydrin TsDHN-2

```
  1  MASYQNRPGA QATDEYGNPM QQLDEYGNPI GGVGATGGGG AGYGTGGGYG
 51  GGATGGEGYG TGALGAGAGA RHHGQEQLHK EGGGGLGGML HRSGSGSSSS
101  SEDDGQGGRR KKGITQKIKE KLPGQHDQSG QSQGMGMGTT TGYDAGGYGG
151  QHHEKKGITD KIKEKLPGQD QSGQSQGMGM GATTGYDAGG YGGERHEKKG
201  MMDKIKDKLP GGGGR
```

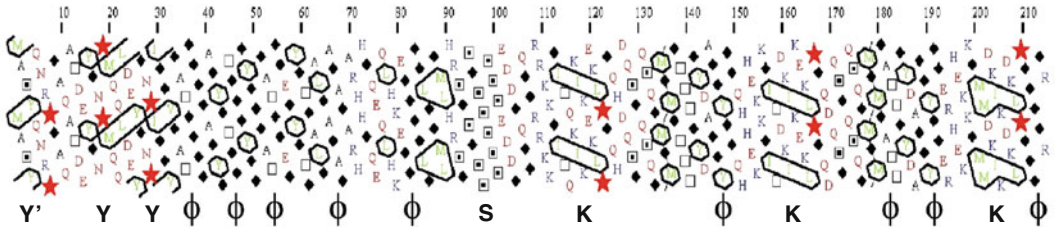

Fig. 1 Amino acid sequences and classification of *Thellungiella salsuginea* dehydrins (**a**) TsDHN-1 (acidic, 267 residues, M_r 30,140.3 Da, theoretical pI 5.25, net charge −19 at neutral pH) and (**b**) TsDHN-2 (basic, 215 residues, M_r 21,435.1 Da, theoretical pI 7.91, net charge +1 at neutral pH). In each *panel*, two representations are used. First, the sequences are given with the following colour scheme: (*red* P and acidic residues D, E, N, Q; *blue* basic residues H, K, R; *green* hydrophobic residues V, L, I, F, W, M, Y; and *black* for all other residues G, S, T, C, A). *Shaded regions* show our interpretation of Y, S, and K motifs for both proteins, with additional glycine-rich φ segments for TsDHN-2. Second, each primary structure representation is visually enhanced via hydrophobic cluster analysis (HCA) (Callebaut et al. 1997; Gaboriaud et al. 1987), using symbols (*opened square* T; *opened square with dot* S; *filled diamond* G; *asterisk* P), and *colours* (*red* P and acidic residues D, E, N, Q; *blue* basic residues H, K, R; *green* hydrophobic residues V, L, I, F, W, M, Y; and *black* for all other residues G, S, T, C, A). The Y, K, S, and φ segments are marked. The Y (consensus sequence (V/T)D (E/Q)YGNP), K (consensus sequence EKKGIMDKIKEKLPG), S (run of 5 or 6 Ser, a phosphorylation sink), and φ (run of polar residues, many Gly) segments are identified. At the amino terminus of each sequence is a Y-like segment that we denote Y′. Dehydrin TsDHN-1 can be classified as S_1K_3, or possibly $Y_1S_1K_4$ if one includes the lysine-rich cluster (denoted K′) that does not exactly match the consensus, and if one includes the Y-like segment (denoted Y′) at the amino-terminus. By the same reasoning, dehydrin TsDHN-2 can be classified as $Y_2S_1K_3\varphi_9$, or possibly $Y_3S_1K_3\varphi_9$. The sequence panels in this figure have been partially adapted from Rahman et al. (2010). This figure is available in *colour* in the web version of the article

Thellungiella halophila) (Wong et al. 2005). This plant is a member of the *Brassicaceae* family and has been proposed as a new model plant for research on abiotic stress tolerance (Amtmann 2009; Griffith et al. 2007; Inan et al. 2004; Pedras and Zheng 2010). The classification of TsDHN-1 (acidic, calculated pI 5.25) is conservatively S_1K_3, or $Y_1S_1K_4$ if one interprets two additional segments more liberally; for TsDHN-2 (slightly basic, calculated pI 7.91), the classification is conservatively $Y_2S_1K_3$ or potentially $Y_3S_1K_3$, with roughly 9 glycine-rich φ segments as well (Fig. 1). The cloning, over-expression, purification, and first characterization of recombinant TsDHN-1 and TsDHN-2 have been recently described (Rahman et al. 2010). These proteins were also shown to undergo partial ordering in association with membranes of various lipid compositions, mimicking the plant plasma, mitochondrial, and chloroplast membranes. Reducing the temperature also appeared to induce and/or stabilize ordered secondary structure.

We extend our first study here by investigating the effects of zinc on the secondary structures of TsDHN-1 and

TsDHN-2 in both free and membrane-associated form (using lipid compositions mimicking the plasma, mitochondrial, and chloroplast membranes). Using circular dichroism (CD) and attenuated total reflection (ATR)-Fourier transform infrared (FTIR) spectroscopy, we demonstrate that membrane- and/or zinc-association significantly increases the proportion of ordered secondary structure in each protein (induced disorder-to-order transition), and further that low temperatures increase the degree of order of each dehydrin. These results support the hypothesis that dehydrins stabilize plant outer and organellar membranes in conditions of reduced water content such as low temperature, and further that zinc sequestration may be an important co-factor in stabilization.

Materials and methods

Materials

Most chemicals were reagent grade and acquired from either Fisher Scientific (Unionville, ON) or Sigma–Aldrich (Oakville, ON). Electrophoresis grade chemicals were purchased from ICN Biomedicals (Costa Mesa, CA) or Bio-Rad Laboratories (Mississauga, ON). Protein over-expression, purification, and reconstitution were performed as previously described (Rahman et al. 2010). The stable isotopic compound D_2O was obtained from Cambridge Isotope Laboratories (C.I.L., Andover, MA). The lipids phosphatidylcholine (PC), phosphatidylethanolamine (PE), 1,2-dimyristoyl-*sn*-glycero-3-[phospho-*rac*-(1-glycerol)] (DMPG), phosphatidylinositol (PI), phosphatidylserine (PS), and cholesterol (Chol) were obtained from Avanti Polar Lipids (Alabaster, AL). The lipids DGDG (digalactosyldiacylglycerol), MGDG (monogalactosyldiacylglycerol), and SQDG (sulfonoquinovosyl diacylglycerol) were obtained from Lipid Products (Nutfield Nurseries, Redhill, Surrey, UK).

Protein over-expression and purification

The TsDHN-1 and TsDHN-2 proteins were purified as previously described (Rahman et al. 2010). Protein preparations were dialyzed extensively against 50 mM ammonium bicarbonate (pH 7.3), which is volatile, and were lyophilized for long-term storage. There were thus no salts in the lyophilized proteins, and they were reconstituted by dissolving them in a suitable buffer. Here, the TsDHN-1 and TsDHN-2 samples were dissolved in HEPES buffer (20 mM HEPES–NaOH, pH 7.3, 100 mM NaCl) at a concentration of 10 mg/ml (0.36 and 0.48 mM, respectively). Since these proteins lacked tryptophanyl residues, the extinction coefficients were exceedingly low and the protein concentration was determined by weighing lyophilized proteins in large scale ($\sim$10 mg) and aliquotting known amounts. Protein solutions were stored at -20°C.

Binding of Zn^{2+} by TsDHN-1 and TsDHN-2: isothermal titration calorimetry

Isothermal titration calorimetry (ITC) experiments were carried out using a VP-ITC instrument from Microcal Inc. (Northampton, MA). Lyophilized variants of TsDHN-1 and TsDHN-2 were dissolved in buffer (20 mM HEPES–NaOH, pH 7.3, 100 mM NaCl), and extensively dialyzed against the same solution (at least 2 changes). Following the dialysis, the protein was filtered (0.22 µm pore size) and the concentration was estimated using a bicinchoninic acid assay (BCA), where TsDHN-1 and TsDHN-2 at known concentrations were used as standards. The stock solutions of 5 mM $ZnCl_2$ or 2.5 mM $ZnCl_2$ were prepared in the same buffer prior to each experiment. Samples were degassed in a Thermovac (Northhampton, MA) at 23°C for 10 min. The Zn^{2+} solution was injected into the sample cell, containing 100 µM of TsDHN-1 or TsDHN-2 variant in the above solution. Typically, for TsDHN-1, the titrations were carried out with a preliminary injection of 2 µl followed by 29 injections of 10 µl of 5 mM $ZnCl_2$, with a 300-s spacing between each injection. For TsDHN-2, the titrations were carried out with a preliminary injection of 3 µl followed by 24 injections of 5 µl of 2.5 mM $ZnCl_2$, and then 17 injections of 7 µl of 2.5 mM $ZnCl_2$, with a 300-s spacing between each injection. All experiments were carried out in triplicate at 23°C.

Before analysis, data from the preliminary 3 µl injections were discarded, and heats of dilution of the ligand into solution of 20 mM HEPES–NaOH, pH 7.3, 100 mM NaCl (in the absence of protein) were subtracted from the Zn^{2+} into TsDHN-1/TsDHN-2 titration experiments. In the analyses presented here, the last several points in the titration curves were fitted with linear regression for the purpose of baseline correction. The corrected data were integrated and plotted as a function of the molar ratio, and the binding isotherms obtained were fitted to the Origin "one set of sites" model for both proteins (Origin 5.0, Microcal) (cf., Majava et al. 2008; Tong et al. 2006; Velazquez-Campoy et al. 2004).

Circular dichroism spectroscopy

The effects of Zn^{2+} on the protein secondary structure in buffer alone (in 20 mM HEPES–NaOH, pH 7.3, 100 mM NaCl) were studied by CD spectroscopy on a JASCO J-815 spectropolarimeter (Japan Scientific, Tokyo), equipped with a re-circulating water bath. The scan rates were 50 nm/min, and the band resolution was 1 nm. The protein

concentration was 1.4 mg/ml (0.047 mM) for TsDHN-1 (M_r = 30.1 kDa), and 1.3 mg/ml (0.06 mM) for TsDHN-2 (M_r = 21.4 kDa). The sample volume was 70 µl in a demountable quartz cuvette with a path-length of 0.01 cm. The CD experiments in the presence of Zn^{2+} were done with a molar protein to Zn^{2+} ratio of 1:10, in order to ensure saturation of all binding sites. The CD spectra were collected from 30 to 5°C with 5°C intervals. Four successive scans were recorded, the sample blank was subtracted, and the scans were averaged. The data averaging and smoothing (using the Savitzky-Golay algorithm) operations were accomplished with OriginPro (Version 8, OriginLab Corporation, Northampton, MA).

Lipid vesicle preparation and protein reconstitution for ATR-FTIR spectroscopy

Various lipid stocks in chloroform or in chloroform:H_2O:methanol (1:2:1 by volume) mixtures were prepared at the desired mass ratio. The solvent was then evaporated under a mild flow of nitrogen gas and subsequently kept under vacuum overnight for complete removal of the residual solvent. Lipid mixtures (10 mg) were rehydrated in 1 ml buffer (20 mM HEPES–NaOH, pH 7.3, 100 mM NaCl) at room temperature overnight with vigorous shaking and three freeze–thaw cycles.

Large unilamellar vesicles (LUVs) were formed by extruding lipid mixtures (61 times at 45°C) through a polycarbonate membrane with a 100-nm pore size. The lipid compositions were chosen to mimic one of the following plant membranes: plasma (PC:PS:PI, 33:47:20 by wt%), mitochondrial (PC:PS:PE:Chol, 27:25:29:20 by wt%), or chloroplast (MGDG:DGDG:SQDG:PC:DMPG:PI, 51:26:7:3:9:1 by wt%) (Harwood 1980). The sizes of vesicles were measured to be approximately 100 nm, using a dynamic light scattering (DLS) Zetasizer Nano-S model ZEN1600 instrument (633 nm "red" laser; Malvern Instruments).

For reconstitution, the desired amount of protein (in 20 mM HEPES–NaOH, pH 7.3, 100 mM NaCl) was added to the LUVs at a lipid-to-protein ratio of 1:1 by weight. The protein-LUV complexes were used within 1 h of preparation for FTIR measurements. The lipid-to-protein ratio was chosen to assure a significant signal-to-noise ratio.

First, 5 mM Zn^{2+} in 20 mM HEPES–NaOH, pH 7.3, 100 mM NaCl was added to the protein solution to achieve a concentration of 0.36 mM for TsDHN-1 and 0.48 mM for TsDHN-2 (to reach the molar zinc to protein ratio of 10:1). After allowing the proteins to interact with Zn^{2+} for 5 min at room temperature, LUVs were added to reach a protein-lipid ratio of 1:1 (wt:wt), followed by a further incubation of 10–15 min at room temperature. After incubation, the protein-LUV complexes (with or without Zn^{2+}) were spun down in a table-top centrifuge at 14,000 rpm (18,000×g) for 1 h. After removing the supernatant, the aggregate was used for ATR-FTIR analysis.

Attenuated total reflection-Fourier transform infrared spectroscopy

The effects of Zn^{2+} on the protein secondary structure when associated with membranes were studied with a Bruker Optics Vertex 70 FTIR spectrometer equipped with a liquid nitrogen-cooled mercury cadmium telluride (MCT) detector. A vertical PIKE MIRacle Micro ATR accessory (PIKE Technologies, Madison, WI) combined with a 1-reflection diamond ATR crystal unit with a diameter of 6 mm was used. The crystal was cleaned by isopropanol, followed by double-distilled H_2O. The crystal surface was dried under nitrogen flow before use. All experiments were conducted at room temperature (~22°C). For each spectrum, 1,000 interferograms were collected and Fourier-transformed to give a resolution of 2 cm^{-1}. To minimize the spectral contributions from atmospheric water vapour, the optic and sample compartments of the spectrometer were purged continuously with dry nitrogen.

Aliquots of about 30 µl of this protein-lipid complex solution were added onto a one-reflection diamond ATR crystal one at a time, followed by 45 min incubation in a desiccator under vacuum to form a dry film. A second layer of deposition was necessary to yield a high signal-to-noise ratio spectrum with the amide I signal around 0.6 O.D. (optical density). Spectra ranging from 950 to 1,750 cm^{-1} were collected while a stream of nitrogen gas, containing rich D_2O vapour, flowed over the sample on the crystal with the aid of a home-built bubbler. The spectra, collected after the complete H_2O/D_2O exchange, were used for secondary structure analysis. The completion of H_2O/D_2O exchange was confirmed when the spectra in the amide II region did not change further. A typical measurement needed about 90 to 120 µg of either TsDHN-1 or TsDHN-2.

ATR-FTIR data analysis

The overlapping bands in the ATR-FTIR spectra were resolved by Fourier self-deconvolution (FSD) using OMNIC software (Thermo Fisher Scientific, Waltham, MA). The bandwidth at half-height was set to 15 cm^{-1}, and the enhancement value was set to 1.8. The number and the location of peaks of the secondary structure components were verified by the second derivative method using the PeakFit program (version 4.12, Seasolve Software Inc., San Jose, CA). The conditions were chosen to minimize the increase in noise, and the appearance of side chain lobes, while achieving maximum band narrowing.

The wavenumbers of these component bands were subsequently used in the PeakFit program as input parameters for curve-fitting analysis of the amide I original spectrum. The parameters were left free to adjust iteratively, with each wavenumber restricted to vary within a range of ± 2 cm^{-1} (Arrondo et al. 1993). The amide I region ($\sim$1,600 to $\sim$1,700 cm^{-1}) arises due to the peptide backbone C=O stretching, and some in-plane N–H bending in a pure H_2O environment. Since all the FTIR measurements were done here in a saturated D_2O environment, the band located between 1,600 and 1,700 cm^{-1} can be considered to be due to C=O stretching only.

Results and discussion

Metal-binding by dehydrins: physiological significance

Hydroxyl peroxyl radicals are generated in plants during environmental stress. Citrus dehydrins are known to have a scavenging role against hydroxyl radicals and peroxyl radicals (Ueda et al. 2003). It has been suggested that citrus dehydrins play this role through metal ion binding (Hara et al. 2005, 2009), by virtue of their enhanced proportion of histidyl residues (Herzer et al. 2003; Kruger et al. 2002; Svensson et al. 2000). The metal-binding activity of the citrus dehydrin CuCOR15 has been studied by immobilized metal affinity chromatography, showing the importance of a double-His and a His-X_3-His motifs (Hara et al. 2005, 2009). It had been previously shown that a double-His motif binds metal ions more strongly than a single His residue (Gusman et al. 2001).

In turn, the physiological significance of metal-binding by dehydrins has been proposed to revolve around DNA-binding. One of the best-characterized DNA-binding motifs is present in the C_2H_2-type zinc finger proteins, of which 176 members have been revealed by *in silico* analysis to be present in *Arabidopsis thaliana* (Englbrecht et al. 2004). Most (about two-thirds) of these proteins are plant-specific. Plant zinc finger domains differ from those found in yeast and animals by being separated by long spacers of various length and sequences, instead of being clustered. They also contain a conserved QALGGH motif (not found in yeast or animals), which has been shown to have a crucial role in DNA binding in vitro.

Although the C_2H_2 type zinc finger proteins are well characterized with regard to their zinc-dependent DNA-binding activity, recent studies have suggested that dehydrins (which are not zinc finger proteins) also have zinc-enhanced DNA-binding activity. For example, five histidine residues near the N-terminus of the tomato abscisic acid stress ripening protein ASR1 were first suggested to be responsible for its DNA-binding, in the absence of any other well-known DNA-binding motif (Kalifa et al. 2004). Subsequently, the central or C-terminal regions were also shown to play a role (Rom et al. 2006). Zinc-dependent DNA-binding activity was also observed in the citrus dehydrin CuCOR15, with other cations (Mg^{2+}, Ca^{2+}, Mn^{2+}) having little or no effect (Goldgur et al. 2007; Hara et al. 2009). Furthermore, zinc induces ordered secondary structure in both the CuCOR15 and Apo-ASR1 dehydrins, further examples of ligand-induced order in IDPs. We concentrate in this study on the interactions of *Thellungiella* dehydrins with zinc in the absence and presence of membranes.

Binding of Zn^{2+} by TsDHN-1 and TsDHN-2: isothermal titration calorimetry

The association of TsDHN-1 or TsDHN-2 with Zn^{2+} was elucidated by isothermal titration calorimetry. Figure 2 presents results from a typical ITC experiment, which was performed in triplicate for each dehydrin protein. In each experimental run, Zn^{2+} was injected into the sample cell containing a known amount of TsDHN-1 or TsDHN-2 to reach the final protein to ligand molar ratio of 1–11 or 1–5, respectively. The Origin Microcal software for isothermal titration calorimetry integrates the areas under the peaks in isothermal titration curves to obtain the change in heat (q_i) associated with ligand injection. Throughout the experiment, the total concentrations of reactants, $[M_1]_T$ and $[M_2]_T$, are known and used as independent variables. Nonlinear regression analysis of q_i, the dependent variable, allows estimation of the thermodynamic parameters (K_a and ΔH and, thus, ΔS) as follows. First, we used the following (Eq. 1):

$$q_i = \mathrm{V}\Delta H\left([M_1M_2]_i - [M_1M_2]_{i-1}\right), \tag{1}$$

where ΔH is the enthalpy of binding of reactants M_1 and M_2 in the constant calorimetric cell volume (V) during titration i. The analytical solution for the concentration of complex M_1M_2 upon titration i is described by Eq. 2:

$$[M_1M_2]_i = \frac{1 + n[M_2]_{T,i}K_a[M_1]_{T,i} - \sqrt{\left(1 + n[M_2]_{T,i}K_a + K_a[M_1]_{T,i}\right)^2 - 4n[M_2]_{T,i}K_a^2[M_1]_{T,i}}}{2K_a} \tag{2}$$

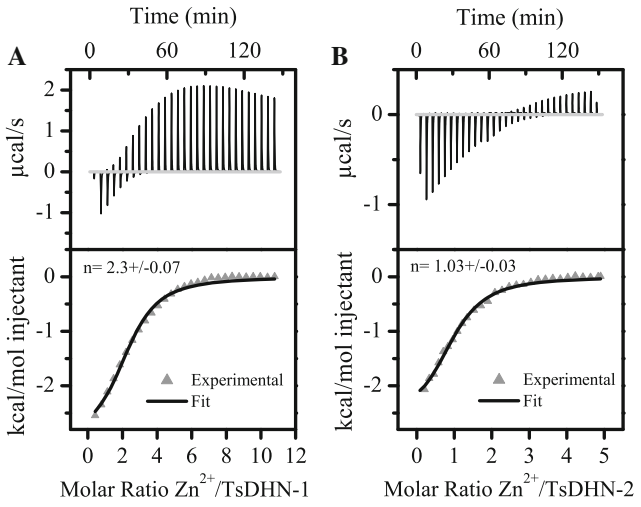

Fig. 2 Isothermal titration calorimetry (ITC) of the interaction of zinc with (**a**) TsDHN-1, and (**b**) TsDHN-2, in 20 mM HEPES–NaOH, pH 7.3, 100 mM NaCl. The isothermal titration calorimetry curves for both proteins were fitted to a model representing one set of binding sites. Thermodynamic parameters thereby derived are given in Tables 1 and 2

where n is the number of independent binding sites, $[M_1]_{T,i}$ and $[M_2]_{T,i}$ are the total concentrations of macromolecule and ligand, respectively, in the cell after injection i. Finally, ΔS is calculated from Eq. 3:

$$\Delta G = -RT \ln K_a = \Delta H - T\Delta S \quad (3)$$

The Origin 5.0 software package (Microcal option) applies the above equations to fit the binding isotherm. The data were fitted to the Origin "one set of sites" model for both proteins, although the "two sets of independent sites" model was also investigated for TsDHN-1 (cf., Majava et al. 2008; Tong et al. 2006; Velazquez-Campoy et al. 2004). The parameters derived from these fittings are summarized in Tables 1 and 2 (Velazquez-Campoy et al. 2004; Wiseman et al. 1989). Standard errors originated from the fitting procedures at the 95% confidence level in the determination of the parameters.

We first describe the data and analysis for TsDHN-1. According to the isothermal titration curve obtained for titration of TsDHN-1 with Zn^{2+}, the binding sites in this protein could not be completely saturated with Zn^{2+} (Fig. 2a). The last six points in the isothermal titration curve were linearly fitted to determine the heat of dilutions and were subtracted from the raw data. Therefore, even though we are confident here about the values for n and K_a that are calculated for TsDHN-1 (Table 1), we do not consider that either the ΔH or $-T\Delta S$ values are reliable (cf., Velazquez-Campoy et al. 2004). These data were fitted to the "one set of sites model", but could also be fitted to a binding model with two sets of binding sites (Tong et al. 2006; Velazquez-Campoy et al. 2004). Here, for simplicity, we present the results only with the "one set of sites model", which yielded $n = 2.3$ (meaning at least 2 zinc ions per protein, and a dissociation constant also in the low-micromolar range, 45 µM. Most probably for TsDHN-1, after the first two sites are saturated, less specific binding of Zn^{2+} occurs.

Dehydrin TsDHN-2 associated with Zn^{2+} at a 1:1 M ratio (Fig. 2b; Table 2). For this protein, the last five points in the isothermal titration curve were linearly fitted to determine the heat of dilutions and were subtracted from the raw data (Fig. 2b). The data were fitted to the Origin "one set of sites" model (Majava et al. 2008), yielding $n = 1.03$ (essentially 1 zinc ion per protein) and a dissociation constant in the low-micromolar range, 26 µM (Table 2). The association was accompanied by a decrease in ΔH and ΔG, suggesting that these interactions are enthalpy driven, and probably predominantly electrostatic. The slight increase of entropy may be due to the release of previously oriented water of solvation (Pierce et al. 1999; Sobhany and Negishi 2006).

Effect of Zn^{2+} on the TsDHN-1 and TsDHN-2 structures: CD spectroscopy

We studied the effects of Zn^{2+} on the secondary structure compositions of TsDHN-1 and TsDHN-2 by CD spectroscopy of the proteins in buffer alone (Figs. 3, 4). There was no detectable precipitation or aggregation of either protein upon addition of cation. At 30°C and in the absence of Zn^{2+}, a deep trough at 197 nm is observed for both TsDHN-1 and TsDHN-2 (Figs. 3a, 4a), indicating that these proteins are mostly random coil under these conditions, with the TsDHN-2 being slightly more ordered than TsDHN-1. This trough shifts towards 205 nm and becomes weaker with decreasing temperature, suggesting a slight cold-stabilization of ordered structure.

Table 1 Thermodynamic parameters for association of TsDHN-1 with Zn^{2+}

n*	K_a (M^{-1})	ΔH (kcal mol^{-1})	$-T\Delta S$ (kcal mol^{-1})
2.3 ± 0.07	(2.2 ± 0.2) × 10^4	−3.04 ± 0.01 (not reliable)	2.8 (not reliable)

Standard errors originated from the fitting procedures at the 95% confidence level in the determination of the parameters

* All three parameters (n, K_a, and ΔH) were iterated to produce the best fit to the experimental data using a model representing one set of binding sites

Table 2 Thermodynamic parameters for association of TsDHN-2 with Zn^{2+}

n*	K_a (M^{-1})	ΔH (kcal mol^{-1})	$-T\Delta S$ (kcal mol^{-1})
1.03 ± 0.03	(3.9 ± 0.4) × 10^4	−2.85 ± 0.11	3.6

Standard errors originated from the fitting procedures at the 95% confidence level in the determination of the parameters

* All three parameters (n, K_a, and ΔH) were iterated to produce the best fit to the experimental data using a model representing one set of binding sites

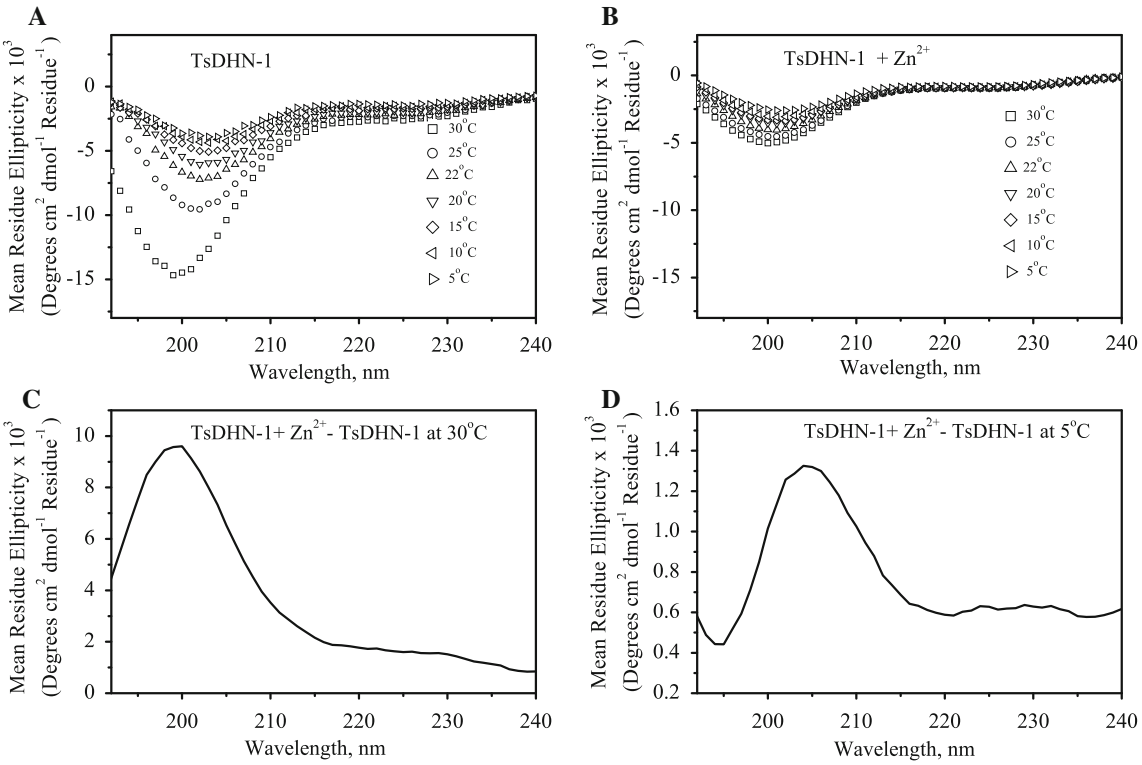

Fig. 3 Solution CD spectra of TsDHN-1 in 20 mM HEPES–NaOH, pH 7.3, 100 mM NaCl, in the **a** absence and **b** presence of Zn^{2+}, at different temperatures. **c**, **d** The differences of CD spectra obtained at 30 and 5°C, respectively (spectrum with zinc minus spectrum without zinc at particular temperature)

For TsDHN-1, in the presence of Zn^{2+}, the CD spectra do not change as dramatically with decreasing temperature as in its absence, suggesting structural stabilization by this cation (compare Fig. 3a with b). In Fig. 3b, the negative minimum at 197 nm is much weaker in the presence of Zn^{2+} than in the absence of Zn^{2+} (Fig. 3a). The difference spectrum (Fig. 3c, obtained by subtracting the spectrum in the absence of Zn^{2+} from the spectrum in the presence of Zn^{2+}), suggests that ordered secondary structures (probably β-turn and β-sheet) are induced in this dehydrin by the presence of Zn^{2+} at 30°C (Fig. 3c). At low temperature, the presence of Zn^{2+} resulted in a redistribution of secondary structure components rather than inducing ordered secondary structures (Fig. 3d).

For TsDHN-2 (Fig. 4b), the addition of Zn^{2+} again rendered the spectra insensitive to temperature. The difference spectra (Fig. 4c, d) obtained by subtracting the spectrum in the absence of Zn^{2+} from the spectrum in the presence of Zn^{2+}, suggest, that in contrast to TsDHN-1, ordered secondary structures are induced at higher temperature, but only redistribution of secondary structures occurs in the presence of Zn^{2+} at lower temperature.

It has become apparent in recent years that the left-handed poly-proline type II (PPII) conformation is an important component of intrinsically disordered proteins (reviewed in Harauz and Libich 2009; Polverini et al. 2008; Rath et al. 2005). The CD spectrum of the poly-proline type II conformation is characterized by a positive maximum at 223 nm and a negative minimum at 197 nm.

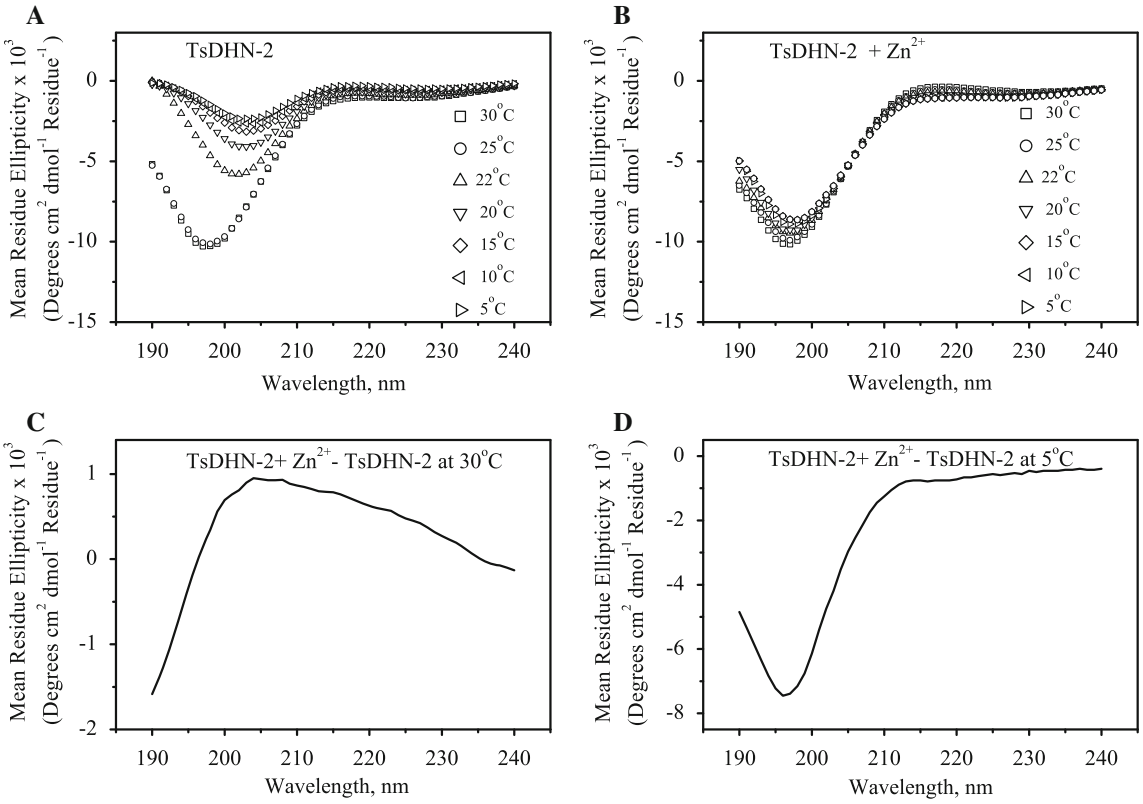

Fig. 4 Solution CD spectra of TsDHN-2 in 20 mM HEPES–NaOH, pH 7.3, 100 mM NaCl, in the **a** absence and **b** presence of Zn^{2+}, at different temperatures. **c**, **d** The differences of CD spectra obtained at 30 and 5°C, respectively (spectrum with zinc minus spectrum without zinc at particular temperature). In the presence of zinc, there is a gain of ordered secondary structure at 30°C under these conditions

However, in many cases the negative minimum due to the α-helical component masks the positive maximum at 223 nm. The PPII conformation is thus best discerned by comparing CD spectra over a range of temperatures (Shi et al. 2002a, b). A temperature-difference spectrum, obtained by subtracting the high-temperature spectrum from the low-temperature one, allows for the "amplification" of the signal from the PPII helix. Here, neither of the difference spectra obtained by subtracting the 30°C spectra from the 5°C spectra of TsDHN-1 and TsDHN-2 (Fig. 5) suggests the presence of the PPII conformation under the particular conditions (pH, temperature, ionic strength) examined here.

Rationale for choice of lipids for LUV preparation

The major plant membrane lipid components are glycolipids and phospholipids, with composition depending on the type of organelle. The plant plasma membrane contains mostly phospholipids, with negligible amounts of other lipids. On the other hand, the predominant lipids in plant chloroplast membranes are glycolipids, or galactolipids such as monogalactosyldiglyceride (MGDG), digalactosyldiglyceride (DGDG), and sulfolipid (SQDG) (Harwood 1980). Different environmental conditions, such as the pH of the soil and low temperature, have been shown to influence the ratio of the galactolipids (Velikova et al. 2002). The presence of galactolipids is crucial for plant growth under normal phosphate-limiting conditions. However, it has been reported that MGDG destabilizes plant lipid during cold stress (Hincha et al. 1998; Novitskaya et al. 2000). The ratio of different lipids also varies depending on the tissue type and affects the activities of enzymes such as phospholipase A (Vishwanath et al. 1996). In this and in our previous study (Rahman et al. 2010), we thus compared the interactions of *Thellungiella* dehydrins with membranes of different lipid compositions in order to gain a broader perspective on their potential roles in different plant cell compartments.

Effect of Zn^{2+} on the membrane-reconstituted TsDHN-1 and TsDHN-2 structures: ATR-FTIR spectroscopy

Since large lipid-protein aggregates cannot be studied by solution CD spectroscopy, ATR-FTIR spectroscopy was

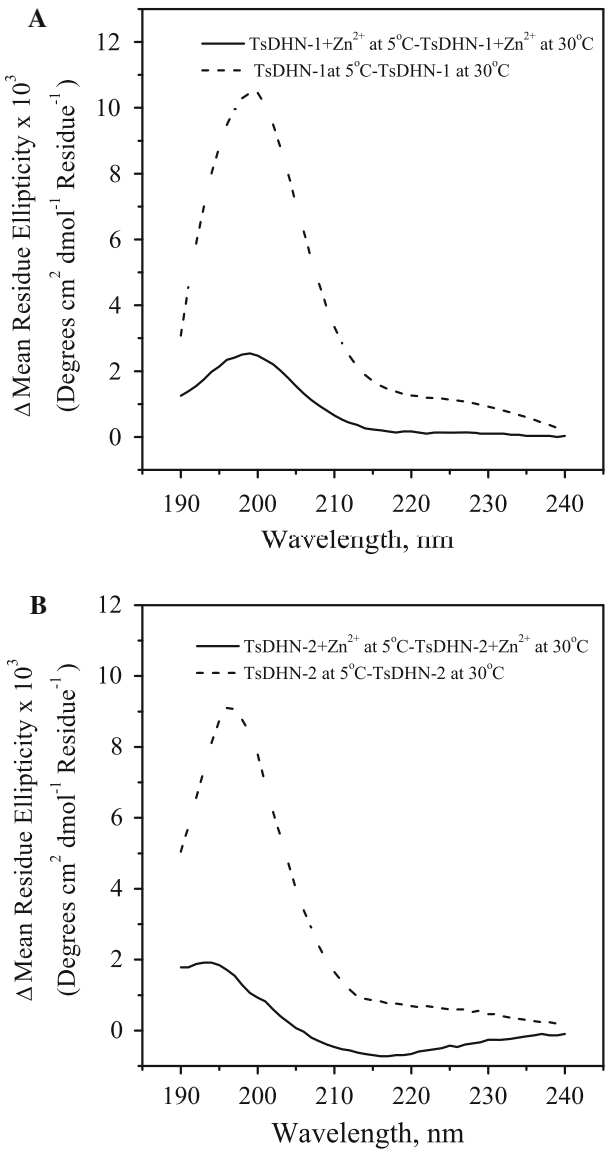

Fig. 5 The differences of solution CD spectra obtained in the presence of zinc at 5 and 30°C (lower temperature spectrum minus higher temperature spectrum) for (**a**) TsDHN-1, and (**b**) TsDHN-2, discounting the presence of a zinc-induced (or zinc-stabilized) polyproline type II (PPII) conformation in TsDHN-1 and TsDHN-2 in solution

applied to study the effect of Zn^{2+} on the membrane-associated TsDHN-1 and TsDHN-2 proteins. The procedure of peak-fitting is illustrated in Fig. 6.

Our first experiment was a control to see the effects of the cation on the lipids alone. The ATR-FTIR spectra of LUVs derived from lipid mixtures mimicking the compositions of plasma, chloroplast, or mitochondrial membranes all collected in the absence of protein, contained ν(C=O), symmetric $\delta(CH_2)$, and asymmetric $\delta(CH_2)$ modes at 1,734, 1,465, and 1,414 cm^{-1}, respectively (Fig. 7a–c). In the presence of Zn^{2+}, an additional peak at 1,593 cm^{-1} was observed. None of the LUV-alone (no protein) spectra showed significant absorption in the amide region, except for that mimicking the mitochondrial membrane (Fig. 7c). For these LUVs, there is a new unique band located at around 1,620 cm^{-1} due to the $\nu(COO^-)$ of PS, which shifts to 1,640 cm^{-1} upon addition of Zn^{2+}. The LUV samples mimicking the composition of plasma and mitochondrial membranes became more compact (condensed acyl chains) upon interaction with Zn^{2+}, due to charge screening, causing them to attach more strongly to the ATR crystal (cf., Smith et al. 2010). This effect is indicated by larger carbonyl lipid peak areas in the presence of Zn^{2+} (Fig. 7a, c).

The addition of Zn^{2+} to either membrane-reconstituted TsDHN-1 or TsDHN-2 caused significant changes in the ATR-FTIR spectra (Figs. 8, 9). All infrared spectra (Figs. 8a–c, 9a–c) were normalized by the carbonyl peak areas after base line corrections. In the presence of Zn^{2+}, TsDHN-1 and TsDHN-2 interact with membranes much less than in its absence, except in the case of TsDHN-2 interacting with LUVs mimicking the composition of the plasma membrane. It has been reported that Zn^{2+} forms bridges between neighbouring negatively charged phospholipid head groups, thus stabilizing the lipid membranes in their gel phase (Binder et al. 2000).

When TsDHN-1 or TsDHN-2 bound to Zn^{2+} comes in contact with lipid membranes, the Zn^{2+} ions are perhaps removed from the proteins and interact instead with the phospholipid head groups, limiting the interactions of the proteins with lipid membranes. For TsDHN-1, peaks at 1,593 cm^{-1} were observed, which might be due to lipids.

In order to determine the effect of Zn^{2+} on the secondary structures of the proteins themselves, the FTIR spectra were corrected for the LUVs background, followed by normalization, such that the area between the linear baseline and the spectra between the region 1,700 and 1,500 cm^{-1} was unity (Figs. 8d–f, 9d–f). The peak at 1,564 cm^{-1} (Fig. 8d, e) or 1,550 cm^{-1} (Fig. 8f), for TsDHN-1, could arise due to the $\nu(COO^-)$ vibration of Glu or Asp side chains, respectively. The peak at 1,575 cm^{-1} for TsDHN-2 (Fig. 9d–f), could arise due to the $\nu(COO^-)$ vibration of Asp side chains. In the presence of Zn^{2+}, the peak at 1,564 cm^{-1} for TsDHN-1 disappears, and instead a peak at 1,605–1,610 cm^{-1} is observed, indicating the involvement of the side chain $\nu(COO^-)$ for interaction with Zn^{2+} (Fig. 8d, e; Mizuguchi et al. 2001; Nara et al. 1995). In addition, peaks at around 1674 cm^{-1} are also observed for plasma

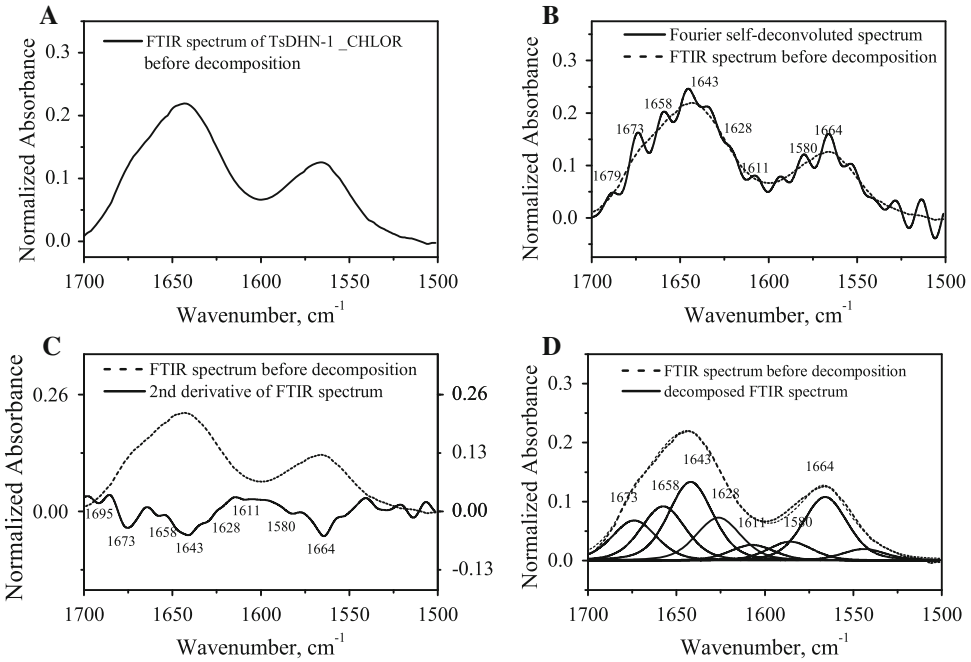

Fig. 6 Demonstration of peak-fitting process for ATR-FTIR spectra. **a** Attenuated total reflection Fourier-transform infrared spectra of TsDHN-2, associated with chloroplast-LUVs at a wt:wt lipid-to-protein ratio of 1:1 in D_2O (*solid line*) at 22°C. **b** Fourier self-deconvolution of an unprocessed ATR-FTIR spectrum of TsDHN-2, associated with chloroplast-LUVs at a wt:wt lipid-to-protein ratio of 1:1 in D_2O at 22°C, using OMNIC software with a bandwidth at a half-height of 15 cm^{-1} and an enhancement value of 1.8. **c** Second derivative of the ATR-FTIR spectrum (**a**) for secondary structure determination by PEAKFIT software. **d** Analysis of the ATR-FTIR spectrum (**a**) for secondary structure determination by PEAKFIT software—the baseline-corrected spectra of the TsDHN-1 and TsDHN-2 proteins reconstituted in LUVs of differing lipid compositions, were deconvoluted using a mixed Gaussian and Lorentzian band shape. Auto-fits of the self-deconvoluted spectra of the original spectra were performed until the coefficient of determination (r^2) was larger than 0.99

membrane or chloroplast membrane reconstituted TsDHN-1 (Fig. 8d, e).

In the FTIR spectra of membrane-reconstituted TsDHN-2, a peak shifted from 1,648 to 1,632 cm^{-1} in the presence of Zn^{2+} suggesting a change in conformation from random coil to β-sheet (Fig. 9d–f; Bandekar 1992; Byler and Susi 1986; Krimm and Bandekar 1986; Surewicz et al. 1993; Surewicz and Mantsch 1988). There was little change observed in the peak located at 1,575 cm^{-1} in the presence of Zn^{2+} for TsDHN-2, suggesting that the side chains of this dehydrin are not involved in interacting with Zn^{2+} to any significant extent (Mizuguchi et al. 2001).

Zinc-induced ordered secondary structure in TsDHN-1 and TsDHN-2

All FTIR spectra were fitted with multiple Gaussian and Lorentzian peaks for detailed secondary structure analysis as illustrated in Fig. 6 and as previously described in detail (Rahman et al. 2010; Smith et al. 2010). Partial overlaps of the amide I band with the deuterated side chain at around 1,564 cm^{-1} for TsDHN-1, and at 1,575 cm^{-1} for TsDHN-2, were observed. Therefore, all peaks located in the region between 1,600 and 1,500 cm^{-1}, after baseline correction, were included during curve fitting. Detailed predictions of the proportions of different types of secondary structures (α-helix, β-strand, and random coil) are given in Tables 3, 4, 5. It should be cautioned that the calculations of overall secondary structure composition from such spectra will vary depending on how peak identification, baseline correction, and peak-fitting are performed. Our method is summarized in Fig. 6. Therefore, we restrict ourselves here to reporting on clear trends, as we have previously done for these dehydrins and for myelin basic protein (Rahman et al. 2010; Smith et al. 2010).

Detailed spectral analysis shows that both TsDHN-1 and TsDHN-2 gain more ordered secondary structure in the presence of Zn^{2+}, particularly β-sheet (Fig. 10). The anti-parallel β-sheet becomes more pronounced in the secondary structure of TsDHN-1, whereas the parallel β-sheet is more pronounced in TsDHN-2. However, the extent in increase of ordered structure is more pronounced for TsDHN-2. For TsDHN-1, there is no significant change in the random coil structure, but there is an

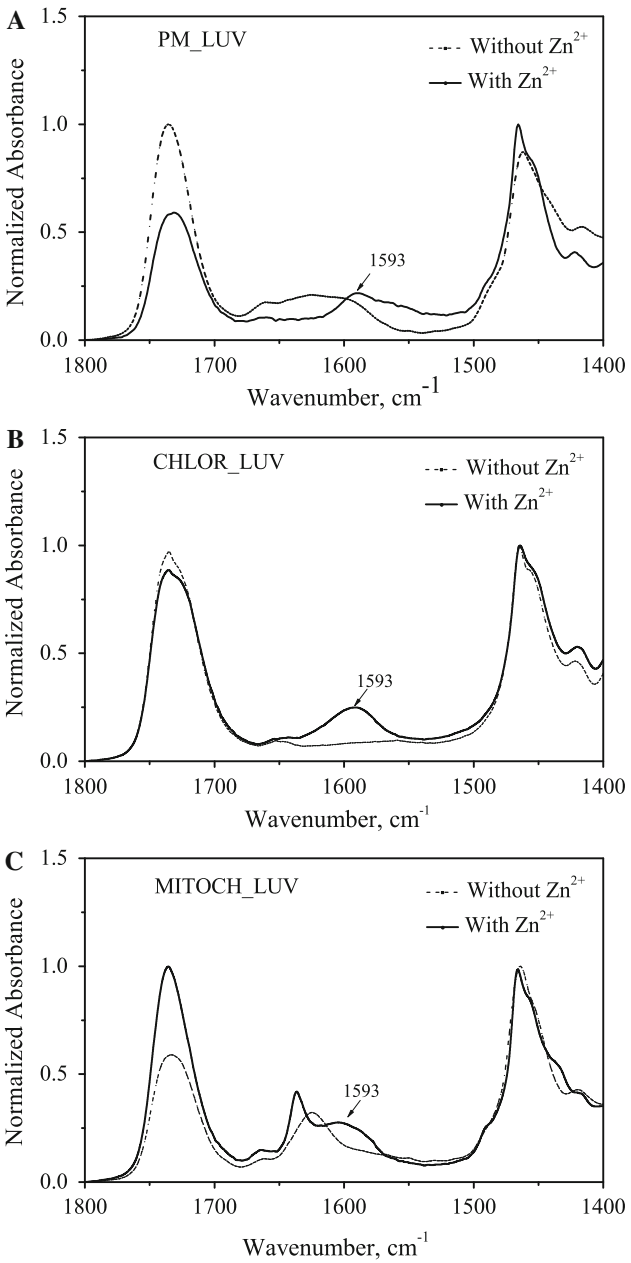

Fig. 7 Effects of Zn^{2+} on ATR-FTIR spectra, absorbance versus wavenumber, at room temperature (22°C), for LUVs alone in the absence of protein. The LUV lipid compositions mimic the plant **a** plasma (PM_LUV), **b** chloroplast (CHLOR_LUV), or **c** mitochondrial (MITOCH_LUV) membranes

increase of turn structures and a decrease in the side chain contributions. Little change in side chain contributions due to Zn^{2+} is observed for TsDHN-2. There is also a synergistic effect of lipid composition, as TsDHN-1 gains more ordered secondary structure when associated with LUVs mimicking the lipid compositions of chloroplast membranes (Fig. 10a, b). The FTIR spectra for TsDHN-1 associated with LUVs mimicking the composition of mitochondria were not of suitable quality for secondary structure analysis with the above method and are not presented.

It has been suggested that dehydrins retain their intrinsically disordered conformation in the formation of hydrogels in conditions of drought, thereby avoiding structural collapse that well-folded proteins would undergo (Mouillon et al. 2008). Our results here demonstrate that dehydrins undergo a disorder-to-order transition in association with membranes and zinc. These new data extend our previous study in which we demonstrated induced order in these same dehydrins upon membrane association at low temperatures (Rahman et al. 2010). Thus, the conformational space sampled by dehydrins in vivo would depend on their particular environment within the cell—the proteins at a membrane interface would be more ordered than those within the bulk hydrogel.

Significance of zinc sequestration by *Th. salsuginea* dehydrins

The sequestration of heavy metals such as zinc has been documented for several LEA proteins and dehydrins (Alsheikh et al. 2003; Heyen et al. 2002; Xu et al. 2008; Zhang et al. 2006). More recently, it has been reported that Zn^{2+} promotes the association of citrus dehydrins with DNA, and that this association was mediated by domains enriched with histidyl and lysyl residues (Hara et al. 2009). This mechanism makes sense since polylysine chains have long been used as a coating to fix DNA to solids (Eisen and Brown 1999), and it is known that His-His or His-X3(4)-His motifs, or combinations thereof, can bind to macromolecules chelating metal ions (such as DNA) through Zn^{2+} intermediates (Vallee and Auld 1995).

Here, TsDHN-1 is an acidic S_1K_3 type dehydrin containing a His-His pair (residues 250 and 251, counting the N-terminal Met as #1) which may play a role in promoting the ordered secondary structure in the presence of Zn^{2+}. In contrast, TsDHN-2 contains two His-His pairs (residues 72 and 73, and 152 and 153), which may play a role in promoting ordered secondary structure in the presence of Zn^{2+}. In addition, the negatively charged side chains in TsDHN-1 may also interact with Zn^{2+}. Previously and independently, studies on *Brassica juncea* dehydrins led to the suggestion that they confer heavy metal tolerance (Xu et al. 2008). Our results here indicate that zinc sequestration by free or membrane-associated *Th. salsuginea* dehydrins results in induced ordered structure, the physiological significance of which remains to be determined. We suggest here that zinc may be important also for membrane-stabilization via dehydrins in plants subjected to extremes of cold or drought.

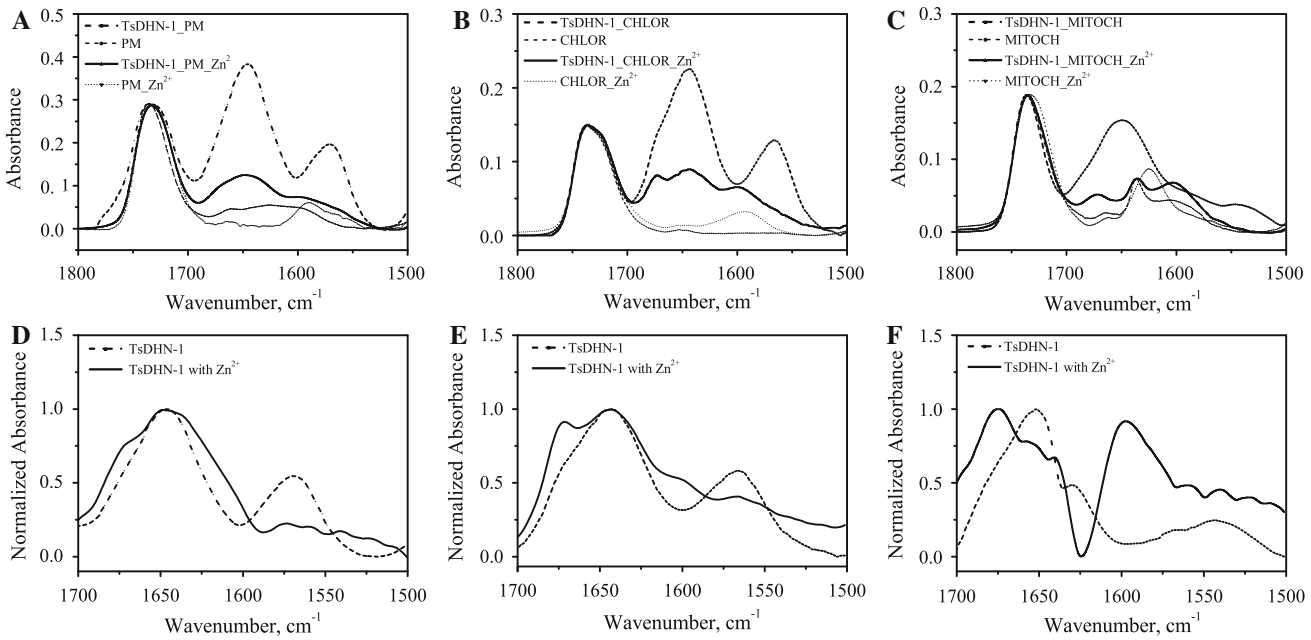

Fig. 8 Effects of Zn^{2+} on ATR-FTIR spectra of TsDHN-1 at room temperature (22°C). In *panels* (**a**–**c**), the protein is membrane-associated with LUV lipid compositions mimicking the plant (**a**) plasma (PM_LUV), **b** chloroplast (CHLOR_LUV), and **c** mitochondrial (MITOCH_LUV) membranes. *Panels* (**d**–**f**) represent the corresponding spectra of protein alone, after subtraction of the lipid spectrum

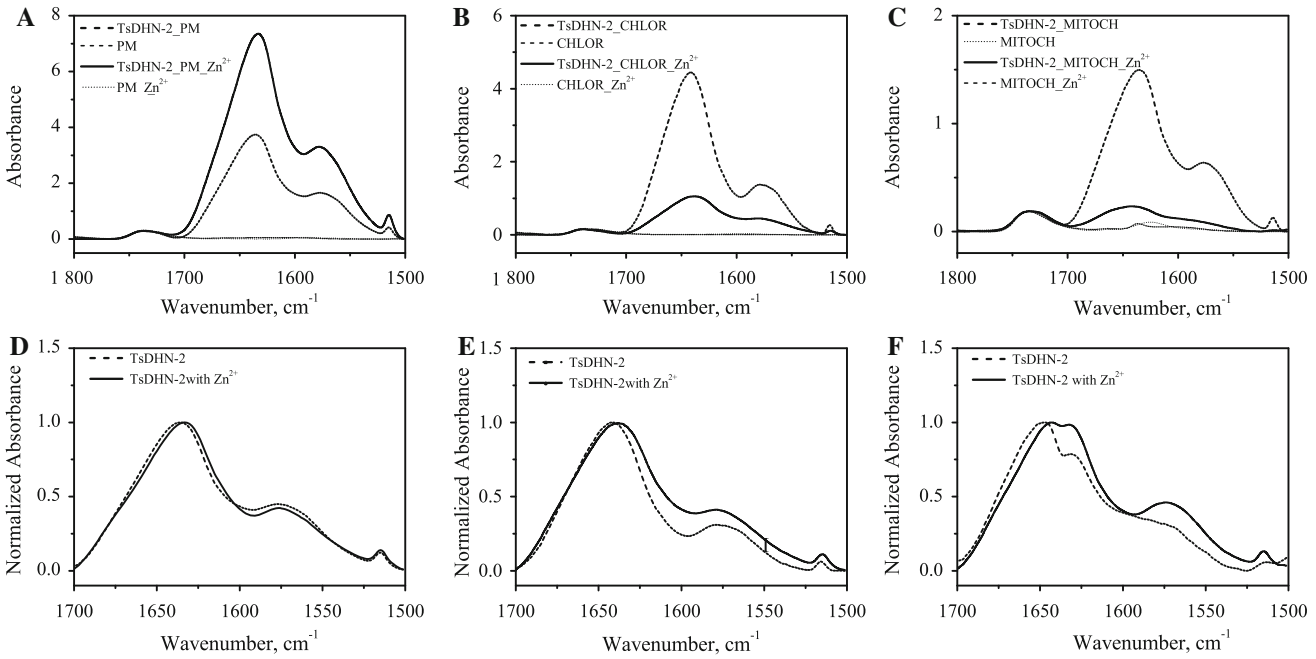

Fig. 9 Effects of Zn^{2+} on ATR-FTIR spectra of TsDHN-2 at room temperature (22°C). In *panels* (**a**–**c**), the protein is membrane-associated with LUV lipid compositions mimicking the plant **a** plasma (PM_LUV), **b** chloroplast (CHLOR_LUV), and **c** mitochondrial (MITOCH_LUV) membranes. *Panels* (**d**–**f**) represent the corresponding spectra of protein alone, after subtraction of the lipid spectrum

Table 3 Effect of zinc on secondary structure components of TsDHN-1 and TsDHN-2 bound to large unilamellar vesicles mimicking the plant plasma membrane (PC:PE:PI at 33:47:20 by wt%), with a 1:10 M ratio of TsDHN-x:Zn^{2+}

Components of TsDHN-1	λ_{max} (cm^{-1})	Absence of Zn^{2+}	Presence of Zn^{2+}	Components of TsDHN-2	λ_{max} (cm^{-1})	Absence of Zn^{2+}	Presence of Zn^{2+}
Side chain contribution				Side chain contribution	1,517	3.3 ± 0.5	2.7 ± 1
Side chain contribution	1,535		6.2 ± 0.7	Side chain contribution	1,546	2.6 ± 0.1	5.2 ± 1
Side chain contribution	1,555	1.3 ± 0.7		Side chain contribution	1,562	7.1 ± 0.1	9.1 ± 1
Side chain contribution	1,565	17.0 ± 1.0	6.4 ± 0.2	Side chain contribution	1,579	11.3 ± 0.2	9.5 ± 0.3
Side chain contribution	1,609	11.3 ± 0.6	7.1 ± 1.1	Side chain contribution	1,609	11.8 ± 0.2	12.6 ± 0.3
β-strand	1,625	12.9 ± 0.2	19.6 ± 0.3	β-strand	1,627	17.2 ± 0.5	25.4 ± 0.5
Random coil	1,647	37.5 ± 0.7	31.5 ± 0.9	Random coil	1,644	28.3 ± 0.6	15.8 ± 4
Turn	1,672	17.8 ± 0.6	23.7 ± 0.5	Turn	1,658		12.4 ± 4
Side chain contribution	1,699	2.4 ± 0.2	5.5 ± 0.4	Turn	1,671	14.0 ± 0.5	5.7 ± 3
				Anti parallel β-strand	1,684	4.3 ± 0.1	2.8 ± 1
Total		100.2%	100.0%			99.9%	101.2%

The columns show the percentage area of each peak, with errors representing the standard deviation of two replicates of data sets. The values will not necessarily add up precisely to 100% because of rounding errors

Table 4 Effect of zinc on secondary structure components of TsDHN-1 and TsDHN-2 bound to large unilamellar lipid vesicles mimicking the plant chloroplast membrane (MGDG:DGDG:SQDG:PC:DMPG:PE:PI at 51:26:7:3:9:1 by wt%), with a 1:10 M ratio of TsDHN-x:Zn^{2+}

Components of TsDHN-1	λ_{max} (cm^{-1})	Absence of Zn^{2+}	Presence of Zn^{2+}	Components of TsDHN-2	λ_{max} (cm^{-1})	Absence of Zn^{2+}	Presence of Zn^{2+}
				Side chain contribution	1,514	1.2 ± 0.5	1.6 ± 4.0
Side chain contribution	1,540–1,543	3.3 ± 0.6	2.7 ± 0	Side chain contribution	1,543		3.5 ± 2.0
Side chain contribution	1,562–1,565	17.8 ± 0.7	6.8 ± 0.3	Side chain contribution	1,562	9.6 ± 1.0	7.2 ± 0.7
Side chain contribution	1,582–1,585	10.5 ± 1.4	5.1 ± 0.4	Side chain contribution	1,578	8.7 ± 2.0	8.8 ± 4.0
Side chain contribution	1,602		10.8 ± 0.2	Side chain contribution	1,596		7.5 ± 3.0
Side chain contribution	1,611–1,614	5.5 ± 0.4	2.4 ± 0.1	Side chain contribution	1,613	8.5 ± 1.0	10.8 ± 0.5
β-strand	1,627–1,628	12.6 ± 1.5	17.2 ± 0.5	β-strand	1,629	13.3 ± 2.0	17.6 ± 1.4
Random coil	1,642–1,645	25.7 ± 1.2	22.4 ± 0.2	Random coil	1,643	25.7 ± 1.0	12.4 ± 2.2
Alpha Helices	1,659	8.9 ± 1.2	7.0 ± 0.3	Alpha Helices	1,651	11.8 ± 1.0	10.7 ± 1.6
Turn	1,671–1,673	15.7 ± 1.2	25.5 ± 0.2	Turn	1,663	13.6 ± 1.7	12.0 ± 1.0
				Anti parallel β-strand	1,679	7.7 ± 1.6	7.8 ± 1.3
Total		100.0%	99.9%			100.1%	100.0%

The columns show the percentage area of each peak, with errors representing the standard deviation of two replicates of datasets. The values will not necessarily add up precisely to 100% because of rounding errors

Conclusions

We have investigated the interactions of *Th. salsuginea* dehydrins TsDHN-1 and TsDHN-2 with Zn^{2+} and membranes, in vitro, to gain further insight into their physiological roles. Using a combination of complementary spectroscopic methods, we have shown that both proteins associate with membranes of different lipid compositions, and thereby gain ordered secondary structure, consistent with other dehydrins that have been investigated (Koag et al. 2003, 2009; Soulages et al. 2002, 2003). These strong membrane interactions of both dehydrins, with concomitant induced folding (ordered secondary structure formation) support the hypothesis that they protect plant plasma and organellar membranes under conditions of extreme cold (Beck et al. 2007; Zhang et al. 2010). Zinc has been shown to stabilize ordered secondary structure in many intrinsically disordered proteins (briefly reviewed in, e.g., Smith et al. 2010). Here, the divalent cation Zn^{2+} has been shown to have a strong stabilizing effect on both dehydrin

Table 5 Effect of zinc on secondary structure components of TsDHN-1 and TsDHN-2 bound to large unilamellar lipid vesicles mimicking the plant mitochondrial membrane (PC:PS:PE:Chol at 27:25:29:20 by wt%), with a 1:10 M ratio of TsDHN-x:Zn^{2+}

Components of TsDHN-2	λ_{max} (cm^{-1})	Absence of Zn^{2+}	Presence of Zn^{2+}
Side chain contribution	1,551	2.9 ± 1.0	3.6 ± 0.2
Side chain contribution	1,567	6.3 ± 0.7	9.4 ± 0.11
Side chain contribution	1,581	5.9 ± 1.0	8.3 ± 0.5
Side chain contribution	1,593	6.3 ± 1.0	3.0 ± 0.6
Side chain contribution	1,611	7.5 ± 0.7	9.1 ± 0.4
β-strand	1,629	19.2 ± 1.0	24.7 ± 1.3
Random coil	1,646	25.7 ± 1.0	19.9 ± 1.5
Turn	1,660	17.4 ± 0.7	14.2 ± 1.5
	1,672		5.5 ± 0.9
β-strand	1,678	9.1 ± 1.0	2.1 ± 0.3
Total		100.3%	99.9%

The columns show the percentage area of each peak, with errors representing the standard deviation of two replicates of datasets. The values will not necessarily add up precisely to 100% because of rounding errors

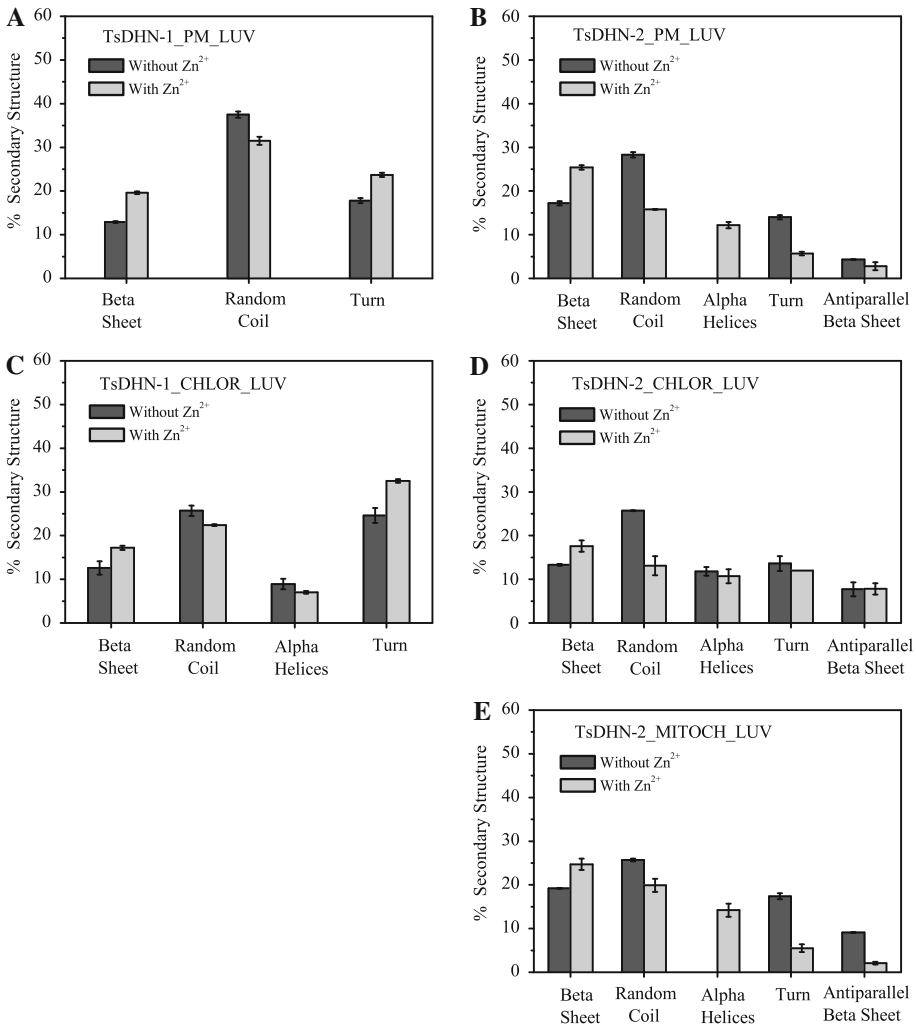

Fig. 10 Effect of Zn^{2+} on secondary structure composition of membrane-associated (**a**, **c**) TsDHN-1, and (**b**, **d**, **e**) TsDHN-2 at room temperature (22°C). The LUV lipid compositions mimic the plant (**a**, **b**) plasma (PM_LUV), (**c**, **d**) chloroplast (CHLOR_LUV), or (**e**) mitochondrial (MITOCH_LUV) membranes. *Error bars* represent the standard deviation of triplicate measurements

structures, both free and in membrane-bound form, indicating a synergistic interaction and potentially a further mechanism for cold-stabilization.

Acknowledgments This work was supported by the Natural Sciences and Engineering Research Council of Canada (G.H.) and initially by the Advanced Food and Materials Network (AFMNet, B.A.M., J.R.D., G.H.), a national Network of Centres of Excellence. J.R.D. acknowledges support from the Canada Research Chair Program. The authors are grateful to Dr. David Libich for assistance with Fig. 1, to Mr. Miguel De Avila for help with the isothermal titration calorimetry and to Dr. Leonid Brown of the University of Guelph for many helpful discussions on FTIR data collection and analysis.

References

Allagulova C, Gimalov FR, Shakirova FM, Vakhitov VA (2003) The plant dehydrins: structure and putative functions. Biochemistry (Moscow) 68:945–951

Alsheikh MK, Heyen BJ, Randall SK (2003) Ion binding properties of the dehydrin ERD14 are dependent upon phosphorylation. J Biol Chem 278:40882–40889

Amtmann A (2009) Learning from evolution: *Thellungiella* generates new knowledge on essential and critical components of abiotic stress tolerance in plants. Mol Plant 2:3–12

Arrondo JL, Muga A, Castresana J, Goni FM (1993) Quantitative studies of the structure of proteins in solution by Fourier-transform infrared spectroscopy. Prog Biophys Mol Biol 59:23–56

Bandekar J (1992) Amide modes and protein conformation. Biochim Biophys Acta 1120:123–143

Battaglia M, Solorzano RM, Hernandez M, Cuellar-Ortiz S, Garcia-Gomez B, Marquez J, Covarrubias AA (2007) Proline-rich cell wall proteins accumulate in growing regions and phloem tissue in response to water deficit in common bean seedlings. Planta 225:1121–1133

Battaglia M, Olvera-Carrillo Y, Garciarrubio A, Campos F, Covarrubias AA (2008) The enigmatic LEA proteins and other hydrophilins. Plant Physiol 148:6–24

Beck EH, Fettig S, Knake C, Hartig K, Bhattarai T (2007) Specific and unspecific responses of plants to cold and drought stress. J Biosci 32:501–510

Binder H, Arnold K, Ulrich AS, Zschörnig O (2000) The effect of Zn(2+) on the secondary structure of a histidine-rich fusogenic peptide and its interaction with lipid membranes. Biochim Biophys Acta 1468:345–358

Bravo LA, Gallardo J, Navarrete A, Olave N, Martinez J, Alberdi M, Close TJ, Corcuera LJ (2003) Cryoprotective activity of a cold-induced dehydrin purified from barley. Physiol Plant 118:262–269

Byler DM, Susi H (1986) Examination of the secondary structure of proteins by deconvolved FTIR spectra. Biopolymers 25:469–487

Callebaut I, Labesse G, Durand P, Poupon A, Canard L, Chomilier J, Henrissat B, Mornon JP (1997) Deciphering protein sequence information through hydrophobic cluster analysis (HCA): current status and perspectives. Cell Mol Life Sci 53:621–645

Campbell SA, Close TJ (1997) Dehydrins: genes, proteins, and associations with phenotypic traits. New Phytol 137:61–74

Caramelo JJ, Iusem ND (2009) When cells lose water: lessons from biophysics and molecular biology. Prog Biophys Mol Biol 99:1–6

Ceccardi TL, Meyer NC, Close TJ (1994) Purification of a maize dehydrin. Protein Expr Purif 5:266–269

Close TJ (1997) Dehydrins: a commonality in the response of plants to dehydration and low temperature. Physiol Plant 100:291–296

Danyluk J, Perron A, Houde M, Limin A, Fowler B, Benhamou N, Sarhan F (1998) Accumulation of an acidic dehydrin in the vicinity of the plasma membrane during cold acclimation of wheat. Plant Cell 10:623–638

Eisen MB, Brown PO (1999) DNA arrays for analysis of gene expression. Methods Enzymol 303:179–205

Englbrecht CC, Schoof H, Bohm S (2004) Conservation, diversification and expansion of C2H2 zinc finger proteins in the *Arabidopsis thaliana* genome. BMC Genomics 5:39

Eom JW, Baker WR, Kintanar A, Wurtele ES (1996) The embryo-specific EMB-1 protein of *Daucus carota* is flexible and unstructured in solution. Plant Sci 115:17–24

Gaboriaud C, Bissery V, Benchetrit T, Mornon JP (1987) Hydrophobic cluster analysis: an efficient new way to compare and analyse amino acid sequences. FEBS Lett 224:149–155

Garay-Arroyo A, Colmenero-Flores JM, Garciarrubio A, Covarrubias AA (2000) Highly hydrophilic proteins in prokaryotes and eukaryotes are common during conditions of water deficit. J Biol Chem 275:5668–5674

Goldgur Y, Rom S, Ghirlando R, Shkolnik D, Shadrin N, Konrad Z, Bar-Zvi D (2007) Desiccation and zinc binding induce transition of tomato abscisic acid stress ripening 1, a water stress- and salt stress-regulated plant-specific protein, from unfolded to folded state. Plant Physiol 143:617–628

Griffith M, Timonin M, Wong AC, Gray GR, Akhter SR, Saldanha M, Rogers MA, Weretilnyk EA, Moffatt B (2007) *Thellungiella*: an *Arabidopsis*-related model plant adapted to cold temperatures. Plant Cell Environ 30:529–538

Gusman H, Lendenmann U, Grogan J, Troxler RF, Oppenheim FG (2001) Is salivary histatin 5 a metallopeptide? Biochim Biophys Acta 1545:86–95

Han B, Hughes DW, Galau GA, Bewley JD, Kermode AR (1997) Changes in late-embryogenesis-abundant (LEA) messenger RNAs and dehydrins during maturation and premature drying of *Ricinus communis* L. seeds. Planta 201:27–35

Hara M, Fujinaga M, Kuboi T (2004) Radical scavenging activity and oxidative modification of *Citrus* dehydrin. Plant Physiol Biochem 42:657–662

Hara M, Fujinaga M, Kuboi T (2005) Metal binding by *Citrus* dehydrin with histidine-rich domains. J Exp Bot 56:2695–2703

Hara M, Shinoda Y, Tanaka Y, Kuboi T (2009) DNA binding of *Citrus* dehydrin promoted by zinc ion. Plant Cell Environ 32:532–541

Harauz G, Libich DS (2009) The classic basic protein of myelin—conserved structural motifs and the dynamic molecular barcode involved in membrane adhesion and protein-protein interactions. Current Protein Pept Sci 10:196–215

Harwood JL (1980) Plant acyl lipids: structure, distribution, and analysis. In: Stumpf PK, Conn EE (eds) Lipids: structure and function. Academic Press, New York, pp 2–56

Herzer S, Kinealy K, Asbury R, Beckett P, Eriksson K, Moore P (2003) Purification of native dehydrin from *Glycine Max* cv., *Pisum sativum*, and *Rosmarinum officinalis* by affinity chromatography. Protein Expr Purif 28:232–240

Heyen BJ, Alsheikh MK, Smith EA, Torvik CF, Seals DF, Randall SK (2002) The calcium-binding activity of a vacuole-associated, dehydrin-like protein is regulated by phosphorylation. Plant Physiol 130:675–687

Hincha DK, Heber U, Schmitt JM (1990) Proteins from frost-hardy leaves protect thylakoids against mechanical freeze-thaw damage in vitro. Planta 180:416–419

Hincha DK, Oliver AE, Crowe JH (1998) The effects of chloroplast lipids on the stability of liposomes during freezing and drying. Biochim Biophys Acta 1368:150–160

Hundertmark M, Hincha DK (2008) LEA (late embryogenesis abundant) proteins and their encoding genes in *Arabidopsis thaliana*. BMC Genomics 9:118

Inan G, Zhang Q, Li P, Wang Z, Cao Z, Zhang H, Zhang C, Quist TM, Goodwin SM, Zhu J, Shi H, Damsz B, Charbaji T, Gong Q, Ma S, Fredricksen M, Galbraith DW, Jenks MA, Rhodes D, Hasegawa PM, Bohnert HJ, Joly RJ, Bressan RA, Zhu JK (2004) Salt cress. A halophyte and cryophyte *Arabidopsis* relative model system and its applicability to molecular genetic analyses of growth and development of extremophiles. Plant Physiol 135:1718–1737

Ismail AM, Hall AE, Close TJ (1999) Purification and partial characterization of a dehydrin involved in chilling tolerance during seedling emergence of cowpea. Plant Physiol 120:237–244

Jepson SG, Close TJ (1995) Purification of a maize dehydrin protein expressed in *Escherichia coli*. Protein Expr Purif 6:632–636

Kalifa Y, Gilad A, Konrad Z, Zaccai M, Scolnik PA, Bar-Zvi D (2004) The water- and salt-stress-regulated Asr1 (abscisic acid stress ripening) gene encodes a zinc-dependent DNA-binding protein. Biochem J 381:373–378

Koag MC, Fenton RD, Wilkens S, Close TJ (2003) The binding of maize DHN1 to lipid vesicles. Gain of structure and lipid specificity. Plant Physiol 131:309–316

Koag MC, Wilkens S, Fenton RD, Resnik J, Vo E, Close TJ (2009) The K-segment of maize DHN1 mediates binding to anionic phospholipid vesicles and concomitant structural changes. Plant Physiol 150:1503–1514

Kosova K, Vitamvas P, Prasil IT (2007) The role of dehydrins in plant response to cold. Biol Plant 51:601–617

Kosova K, Holkova L, Prasil IT, Prasilova P, Bradacova M, Vitamvas P, Capkova V (2008) Expression of dehydrin 5 during the development of frost tolerance in barley (*Hordeum vulgare*). J Plant Physiol 165:1142–1151

Kovacs D, Kalmar E, Torok Z, Tompa P (2008) Chaperone activity of ERD10 and ERD14, two disordered stress-related plant proteins. Plant Physiol 147:381–390

Krimm S, Bandekar J (1986) Vibrational spectroscopy and conformation of peptides, polypeptides, and proteins. Adv Protein Chem 38:181–364

Kruger C, Berkowitz O, Stephan UW, Hell R (2002) A metal-binding member of the late embryogenesis abundant protein family transports iron in the phloem of *Ricinus communis* L. J Biol Chem 277:25062–25069

Lisse T, Bartels D, Kalbitzer HR, Jaenicke R (1996) The recombinant dehydrin-like desiccation stress protein from the resurrection plant *Craterostigma plantagineum* displays no defined three-dimensional structure in its native state. Biol Chem 377:555–561

Majava V, Petoukhov MV, Hayashi N, Pirila P, Svergun DI, Kursula P (2008) Interaction between the C-terminal region of human myelin basic protein and calmodulin: analysis of complex formation and solution structure. BMC Struct Biol 8:10

Mizuguchi M, Fujisawa R, Nara M, Nitta K, Kawano K (2001) Fourier-transform infrared spectroscopic study of Ca2+-binding to osteocalcin. Calcif Tissue Int 69:337–342

Mohan A, Uversky VN, Radivojac P (2009) Influence of sequence changes and environment on intrinsically disordered proteins. PLoS Comput Biol 5:e1000497

Mouillon JM, Gustafsson P, Harryson P (2006) Structural investigation of disordered stress proteins. Comparison of full-length dehydrins with isolated peptides of their conserved segments. Plant Physiol 141:638–650

Mouillon JM, Eriksson SK, Harryson P (2008) Mimicking the plant-cell interior under water stress by macromolecular crowding: Disordered dehydrin proteins are highly resistant to structural collapse. Plant Physiol 148:1925–1937

Nara M, Tanokura M, Yamamoto T, Tasumi M (1995) A comparative study of the binding effects of Mg^{2+}, Ca^{2+}, Sr^{2+}, and Cd^{2+} on calmodulin by Fourier-transform infrared-spectroscopy. Biospectroscopy 1:47–54

Novitskaya GV, Suvorova TA, Trunova TI (2000) Lipid composition of tomato leaves as related to plant cold tolerance. Russ J Plant Physiol 47:728–733

Pedras MS, Zheng QA (2010) Metabolic responses of *Thellungiella halophila/salsuginea* to biotic and abiotic stresses: metabolite profiles and quantitative analyses. Phytochemistry 71:581–589

Pierce MM, Raman CS, Nall BT (1999) Isothermal titration calorimetry of protein-protein interactions. Methods 19:213–221

Polverini E, Rangaraj G, Libich DS, Boggs JM, Harauz G (2008) Binding of the proline-rich segment of myelin basic protein to SH3-domains—spectroscopic, microarray, and modelling studies of ligand conformation and effects of post-translational modifications. Biochemistry 47:267–282

Puhakainen T, Hess MW, Makela P, Svensson J, Heino P, Palva ET (2004) Overexpression of multiple dehydrin genes enhances tolerance to freezing stress in *Arabidopsis*. Plant Mol Biol 54:743–753

Rahman LN, Chen L, Nazim S, Bamm VV, Yaish MWF, Moffatt BA, Dutcher JR, Harauz G (2010) Interactions of intrinsically disordered *Thellungiella salsuginea* dehydrins TsDHN-1 and TsDHN-2 with membranes—synergistic effects of lipid composition and temperature on secondary structure. Biochem Cell Biol 88(5):791–807

Rajesh S, Manickam A (2006) Prediction of functions for two LEA proteins from mung bean. Bioinformation 1:133–138

Rath A, Davidson AR, Deber CM (2005) The structure of "unstructured" regions in peptides and proteins: role of the polyproline II helix in protein folding and recognition. Biopolymers 80:179–185

Rom S, Gilad A, Kalifa Y, Konrad Z, Karpasas MM, Goldgur Y, Bar-Zvi D (2006) Mapping the DNA- and zinc-binding domains of ASR1 (abscisic acid stress ripening), an abiotic-stress regulated plant specific protein. Biochimie 88:621–628

Rorat T, Szabala BM, Grygorowicz WJ, Wojtowicz B, Yin Z, Rey P (2006) Expression of SK(3)-type dehydrin in transporting organs is associated with cold acclimation in *Solanum* species. Planta 224:205–221

Shi Z, Olson CA, Rose GD, Baldwin RL, Kallenbach NR (2002a) Polyproline II structure in a sequence of seven alanine residues. Proc Natl Acad Sci USA 99:9190–9195

Shi Z, Woody RW, Kallenbach NR (2002b) Is polyproline II a major backbone conformation in unfolded proteins? Adv Protein Chem 62:163–240

Smith GST, Chen L, Bamm VV, Dutcher JR, Harauz G (2010) The interaction of zinc with membrane-associated 18.5 kDa myelin basic protein: an attenuated total reflectance-Fourier transform infrared spectroscopic study. Amino Acids 39:739–750

Sobhany M, Negishi M (2006) Characterization of specific donor binding to alpha1, 4-N-acetylhexosaminyltransferase EXTL2 using isothermal titration calorimetry. Methods Enzymol 416:3–12

Soulages JL, Kim K, Walters C, Cushman JC (2002) Temperature-induced extended helix/random coil transitions in a group 1 late embryogenesis-abundant protein from soybean. Plant Physiol 128:822–832

Soulages JL, Kim K, Arrese EL, Walters C, Cushman JC (2003) Conformation of a group 2 late embryogenesis abundant protein from soybean. Evidence of poly (L-proline)-type II structure. Plant Physiol 131:963–975

Steponkus PL, Uemura M, Joseph RA, Gilmour SJ, Thomashow MF (1998) Mode of action of the COR15a gene on the freezing

tolerance of *Arabidopsis thaliana*. Proc Natl Acad Sci USA 95:14570–14575

Surewicz WK, Mantsch HH (1988) New insight into protein secondary structure from resolution-enhanced infrared spectra. Biochim Biophys Acta 952:115–130

Surewicz WK, Mantsch HH, Chapman D (1993) Determination of protein secondary structure by Fourier transform infrared spectroscopy: a critical assessment. Biochemistry 32:389–394

Svensson J, Palva ET, Welin B (2000) Purification of recombinant *Arabidopsis thaliana* dehydrins by metal ion affinity chromatography. Protein Expr Purif 20:169–178

Thalhammer A, Hundertmark M, Popova AV, Seckler R, Hincha DK (2010) Interaction of two intrinsically disordered plant stress proteins (COR15A and COR15B) with lipid membranes in the dry state. Biochim Biophys Acta 1798:1812–1820

Tolleter D, Jaquinod M, Mangavel C, Passirani C, Saulnier P, Manon S, Teyssier E, Payet N, Avelange-Macherel MH, Macherel D (2007) Structure and function of a mitochondrial late embryogenesis abundant protein are revealed by desiccation. Plant Cell 19:1580–1589

Tolleter D, Hincha DK, Macherel D (2010) A mitochondrial late embryogenesis abundant protein stabilizes model membranes in the dry state. Biochim Biophys Acta 1798:1926–1933

Tompa P, Kovacs D (2010) Intrinsically disordered chaperones in plants and animals. Biochem Cell Biol 88:167–174

Tompa P, Banki P, Bokor M, Kamasa P, Kovacs D, Lasanda G, Tompa K (2006) Protein-water and protein-buffer interactions in the aqueous solution of an intrinsically unstructured plant dehydrin: NMR intensity and DSC aspects. Biophys J 91:2243–2249

Tong KI, Katoh Y, Kusunoki H, Itoh K, Tanaka T, Yamamoto M (2006) Keap1 recruits Neh2 through binding to ETGE and DLG motifs: characterization of the two-site molecular recognition model. Mol Cell Biol 26:2887–2900

Tunnacliffe A, Wise MJ (2007) The continuing conundrum of the LEA proteins. Naturwissenschaften 94:791–812

Ueda EK, Gout PW, Morganti L (2003) Current and prospective applications of metal ion-protein binding. J Chromatogr A 988:1–23

Uversky VN (2009) Intrinsically disordered proteins and their environment: Effects of strong denaturants, temperature, pH, counter ions, membranes, binding partners, osmolytes, and macromolecular crowding. Protein J 28:305–325

Vallee BL, Auld DS (1995) Zinc metallochemistry in biochemistry. EXS 73:259–277

Velazquez-Campoy A, Leavitt SA, Freire E (2004) Characterization of protein-protein interactions by isothermal titration calorimetry. Methods Mol Biol 261:35–54

Velikova V, Ivanova A, Yordanov I (2002) Changes in lipid compistion of *Phaseolus vulgaris* leaves after simulating acid rain treatment. Bulg J Plant Physiol 28:59–65

Vishwanath BS, Eichenberger W, Frey FJ, Frey BM (1996) Interaction of plant lipids with 14 kDa phospholipase A2 enzymes. Biochem J 320(Pt 1):93–99

Vucetic S, Xie H, Iakoucheva LM, Oldfield CJ, Dunker AK, Obradovic Z, Uversky VN (2007) Functional anthology of intrinsic disorder. 2. Cellular components, domains, technical terms, developmental processes, and coding sequence diversities correlated with long disordered regions. J Proteome Res 6:1899–1916

Wise MJ, Tunnacliffe A (2004) POPP the question: what do LEA proteins do? Trends Plant Sci 9:13–17

Wiseman T, Williston S, Brandts JF, Lin LN (1989) Rapid measurement of binding constants and heats of binding using a new titration calorimeter. Anal Biochem 179:131–137

Wolkers WF, McCready S, Brandt WF, Lindsey GG, Hoekstra FA (2001) Isolation and characterization of a D-7 LEA protein from pollen that stabilizes glasses in vitro. Biochim Biophys Acta 1544:196–206

Wong CE, Li Y, Whitty BR, Diaz-Camino C, Akhter SR, Brandle JE, Golding GB, Weretilnyk EA, Moffatt BA, Griffith M (2005) Expressed sequence tags from the Yukon ecotype of *Thellungiella* reveal that gene expression in response to cold, drought and salinity shows little overlap. Plant Mol Biol 58:561–574

Xie H, Vucetic S, Iakoucheva LM, Oldfield CJ, Dunker AK, Obradovic Z, Uversky VN (2007a) Functional anthology of intrinsic disorder. 3. Ligands, post-translational modifications, and diseases associated with intrinsically disordered proteins. J Proteome Res 6:1917–1932

Xie H, Vucetic S, Iakoucheva LM, Oldfield CJ, Dunker AK, Uversky VN, Obradovic Z (2007b) Functional anthology of intrinsic disorder. 1. Biological processes and functions of proteins with long disordered regions. J Proteome Res 6:1882–1898

Xu J, Zhang YX, Wei W, Han L, Guan ZQ, Wang Z, Chai TY (2008) BjDHNs confer heavy-metal tolerance in plants. Mol Biotechnol 38:91–98

Zhang Y, Li J, Yu F, Cong L, Wang L, Burkard G, Chai T (2006) Cloning and expression analysis of SKn-type dehydrin gene from bean in response to heavy metals. Mol Biotechnol 32:205–218

Zhang C, Ding Z, Xu X, Wang Q, Qin G, Tian S (2010) Crucial roles of membrane stability and its related proteins in the tolerance of peach fruit to chilling injury. Amino Acids 39:181–194

Zhu B, Choi DW, Fenton R, Close TJ (2000) Expression of the barley dehydrin multigene family and the development of freezing tolerance. Mol Gen Genet 264:145–153